ИНСТИТУТ ЯДЕРНОЙ ФИЗИКИ СО АН СССР

G.F. Abdrashitov, A.V. Beloborodov, V.I. Volosov,
V.V. Kubarev, Yu.S. Popov, Yu.N. Yudin

HOT ROTATING PLASMA (PSP-2 EXPERIMENT)

PREPRINT 89-109

НОВОСИБИРСК

Institute of Nuclear Physics

G.F. Abdrashitov, A.V. Beloborodov, V.I. Volosov,
V.V. Kubarev, Yu.S. Popov, Yu.N. Yudin

HOT ROTATING PLASMA
(PSP-2 EXPERIMENT)

PREPRINT 89-109

NOVOSIBIRSK
1989

Hot Rotating Plasma
(PSP-2 Experiment)

G.F. Abdrashitov, A.V. Beloborodov, V.I. Volosov, V.V. Kubarev, Yu.S. Popov, Yu.N. Yudin

Institute of Nuclear Physics
630090, Novosibirsk 90, USSR

ABSTRACT

Studies have been made of the MHD-stable rotating plasma with the parameters: mean energy of ions up to 40 keV in the laboratory frame of reference or up to 20 keV in rotating frame reference, plasma density $3 \cdot 10^{11}$ cm^{-3} (and up to 10^{12} cm^{-3} in special regimes), mean energy of electrons 0.1—1.0 keV (non-Maxwellian spectrum), life-time of particles 10^{-4} s (determined by the charge exchange), and plasma volume 0.1 m^3, in experiments of the PSP-2 device.

The field strength on the plasma was about 20 kV/cm, and the total voltage achieved 0.5 MV. The MHD stabilization conditions are in agreement with the theoretical estimates.

A hot plasma was created in a high-voltage $E \times B$ discharge, the cold hydrogen gas having been puffed without any heating and plasma injection systems.

INTRODUCTION

The experiments described below were intended to solve a number of fundamental problems associated with the creation of thermonuclear systems on the basis of a rotating plasma trap, as well as to investigate analogous systems with a number of full-scale parameters. The experiments were performed on the PSP-2 device [1—3] —one of the modifications of similar systems—the rotating plasma trap using an electrode system placed within the mirror region.

The most important problems in setting up the PSP-2 experiments were:

1. Applications of the total radial potentials (U_t) up to 0.5—1 MV (up to 5—10 MV in a reactor) to a plasma. Similar plasma was earlier studied at no more than 20—30 kV total voltages [4—6];

2. Production of a highly-ionized rotating plasma in the quasi-stationary mode of operation. The nesessary condition for this is enough high energy of ions, $\bar{W}_i > 20 \div 30$ keV, and, as a consequence, enough high value of U_t ($U_t > 0.2 \div 0.3$ MV) at $a/\rho_i \gg 1$ (a radial size of the plasma, ρ_i—ion Larmor radius).

3. Production of an MHD stable plasma. It was assumed that the MHD stabilization of a plasma was achieved under a simultaneous action of two factors: a) stabilization with the aid of longitudinal electron losses and b) stabilization attributed to the slipping of the plasma layers over the radius $\partial \Omega_E / \partial r \neq 0$ («electric shear» $\Omega_E = V_E / r$, $V_E = cE/B$), see [1].

It is the above problems that determined the basic stages of these experiments.

1. PSP-2 DEVICE

The PSP-2 device is an open magnetic trap with a radial electric field (see Figs 1, 2); the physical principles of this system are stated in [1]. The electric field in the plasma volume is generated by two identical systems of ring electrodes placed near the magnetic mirrors (24 electrodes) and by an outer and an inner liners restricting the plasma. The liner surface coincides with the magnetic surfaces of the trap. In the first system of ring electrodes which connects a high-voltage unit to a plasma («active» system) each pair of electrodes has an independent high-voltage power supply. The second system is «passive», there are 68 MOhm resistors between pairs of electrodes. The plasma dimensions in the central plane are $r_1 = 32$ cm and $r_2 = 51$ cm, and the mirrors are 160 cm distant. The surface of the inner liner looks like a lattice consisting of titanium rings to avoid the S-discharge (see Ref. [3]). A ring is 50—70 mm high and 0.5 mm thick, and the rings are at a distance of about 10 mm from each other.

In the $E \times B$ discharge, the plasma is created due to ionization and heating in the crossed fields. Hydrogen leaks into the chamber through 6 puff valves equally spaced throughout the azimuth in the middle of the trap.

The parameters of the device used in these experiments were: magnetic field in the central plane: $B_z = 8 \div 10$ kG, mirror ratio: 2.4; total voltage applied to the plasma: up to 450 kV (up to 500 kV at the electrodes without the dense plasma); the full energy storage in a HV storage unit: about 100 kJ, the capacitance of each level was 20 μF. The initial vacuum, $1 \cdot 10^{-7}$ torr, was provided by a built-in cryogenic pump and by two others placed outside; these pumps utilize overcooled helium. The pumping rate is $5 \cdot 10^4$ l/s and $5 \cdot 10^3$ l/s, respectively.

The hydrogen-plasma experiments were made in the pulse regime. The time-table of each shot was: the capacitors of the storage unit are first charged ($t_s = -100$ s, t_s—the time of switching on), the current appears in magnetic coils ($t_s = -20$ s). After that, hydrogen fills the chamber ($t_s = -0.5 \div 1.0 \cdot 10^{-3}$ s and the thyristor keys are switched on ($t = 0$) forming the electrode voltage.

The arrangement of diagnostic instruments is shown in Fig. 2.

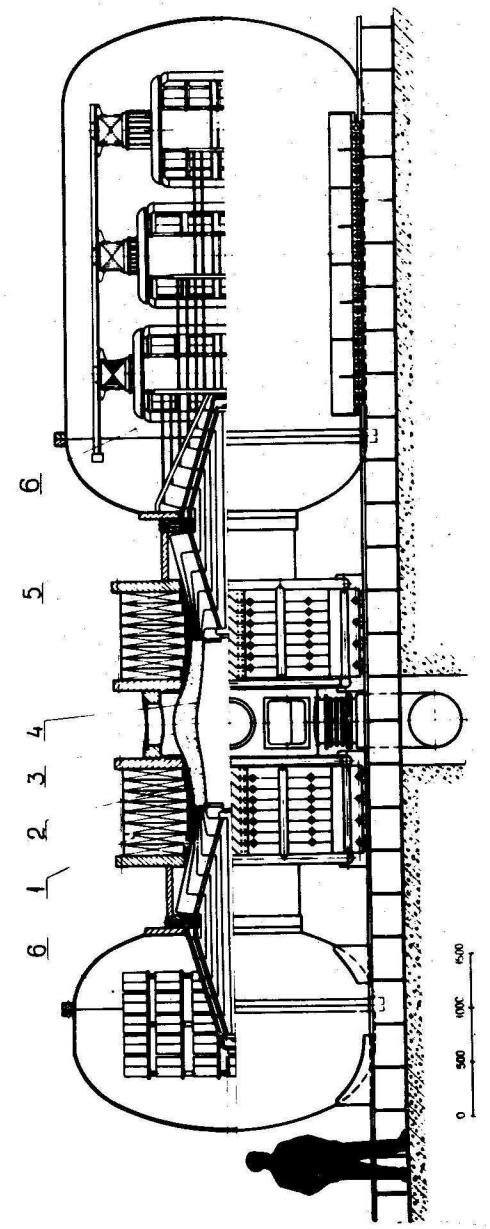

Fig. 1. PSP-2 in section:
1—magnetic field coils; *2*—plasma region; *3*—outer liner; *4*—inner liner; *5*—electrode system; *6*—HV-unit.

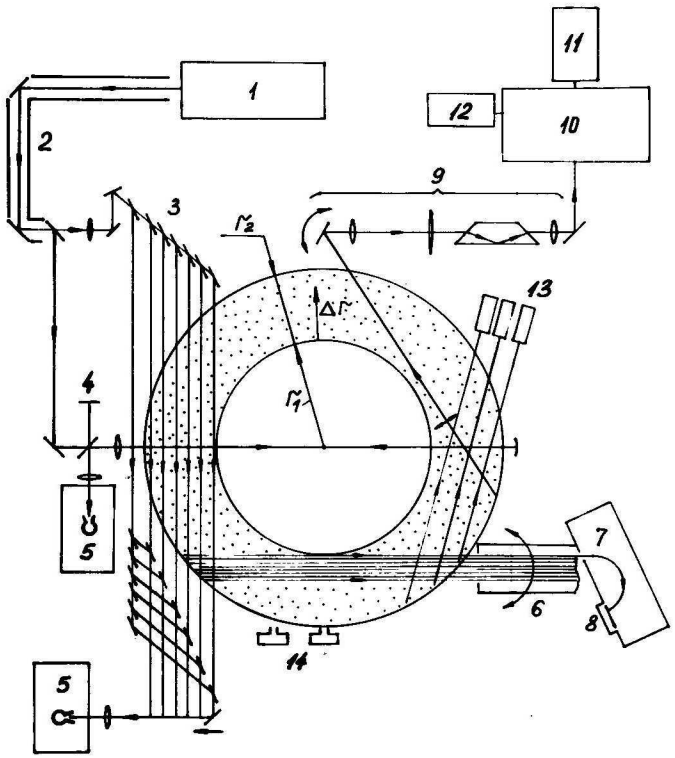

Fig. 2. Arrangement of the diagnostic apparatus in the $z=0$ plane:
Submillimeter interferometer (*1—5*): *1*—HCN-laser, *2*—wave guide, *3*—chord interferometer, *4*—radial interferometer, *5*—InSb detectors; **neutrals analyzer** (*6—8*): *6*—gas stripping cell, *7*—analyzer chamber, *8*—microchannel plate; **optical system** (*9—12*), *9*—collimator, *10*—monochromator, *11*—photomultiplier, *12*—dissector; *13*—**secondary emission detectors**; *14*—**penning cells**.

2. EXPERIMENTAL DATA

Although the maximum parameters of the plasma were rather high (plasma density: $1\cdot10^{12}$ см$^{-3}$, 20 keV ion energy in the rotating frame of reference), we used the regimes with moderate parameters for long-in-time and repeatable experiments (several thousands of shots).

2.1. Plasma Density

The plasma density was measured by a highly-sensitive ($(n\cdot l)_{\min}\simeq4\cdot10^{11}$ cm^{-2}) multichannel HCN-interferometer [9, 10]. The plasma was investigated along one radial and six chordic directions in the central plane of the trap (Fig. 2). In this case, the radial channel of the interferometer determined the mean, plasma density, and the results of the chordic measurements enabled one to reconstruct the density profile $n(r)$ [10]. The average plasma densities, both the measured and the calculated from the reconstructed distributions, coincided within the measurement errors. The typical computer oscillograms $n(t)$ are given in Fig. 3 for $U_s=330$ kV ($U_S=U_T(t=0)$). There is a quasi-stationary region where $n(t)\simeq$ $\simeq$ const.

The discharge was ignited in 0.5 to 0.7 ms after the gas puffing, and then, in 0.5 to 1.0 ms it stopped without any residual currents and breakdowns in the plasma, with the electrode voltage practically recovered.

Spacial plasma density distributions $n(r)$ are presented in Fig. 4 for different moments of time and for different values of U_S. On the radial plasma density distribution we can distinguish two main regions: the 3—5 cm wide region near the outer «positive» liner where the plasma density is several times lower than the average one, and the central region (closer to the inner «negative» liner) where an exponential increasing of density occurs as the distance from the outer liner grows (a dicrease of r). Between these regions, near the point $r=r^*$ ($\Delta r\simeq13$ cm) there is an area of decreasing the density. The maximum density is achieved at a distance equal to 2—3 Larmor radii from the inner liner. As the total voltage, applied to the plasma, increases up to 300—330 kV, the average and the maximum plasma densities grow; at higher voltage the change is insignificant. The problems associated with the density profile and with

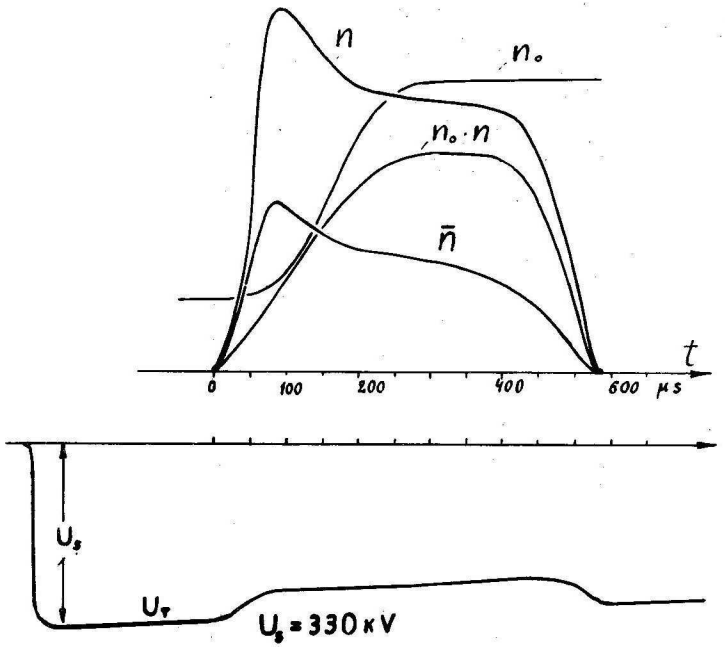

Fig. 3. Oscillograms:
$\bar{n}(t)$ — mean plasma density; $n(t)$, $n_0)(t)$, $n_0 n$ — plasma and neutral-gas densities near the inner liner; $U_t(t)$ — total voltage.

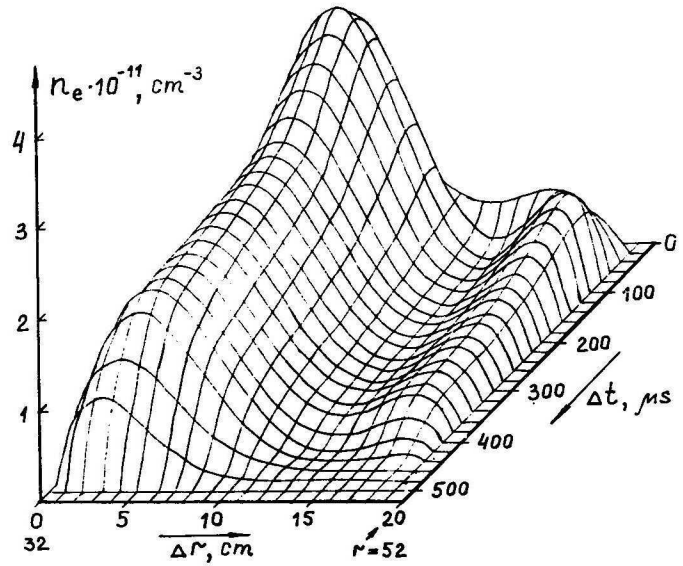

Fig. 4.1. Time resolved plasma density radial profiles in regime $U_S = 330$ kV.

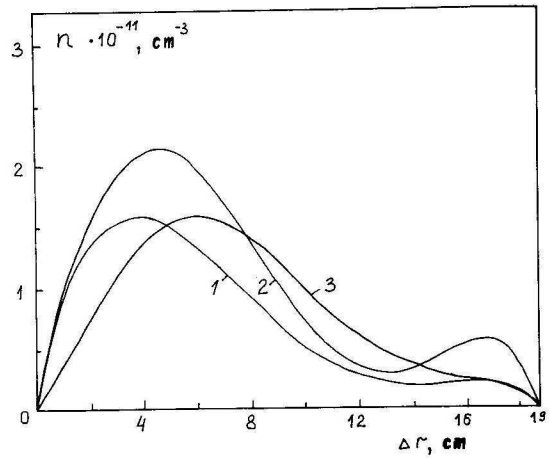

Fig. 4.2. Radial distributions of the plasma density at the onset of the steady-state phase of the discharge ($t = 200$ μs —) for various regimes:
$U_S = 270$ kV (*1*), $U_S = 330$ kV (2), $U_S = 360$ kV(*3*).

the dependence of the average density on the total voltage are treated in more detail is Sec. 3.1.

2.2. Potentials and Currents in a Plasma

We controlled over the following parameters of the discharge: total plasma voltage U_T, voltage U_N at each pair of electrodes (23 detectors), current J_N, flowing to the plasma from each electrode (11 probes at odd levels), and current I_N flowing between the levels (12 probes at odd levels).

The discharge is powered by a rectifier-storage unit, one of the section of which is schematically shown in Fig. 5. This figure also shows the arrangement of the basic current and voltage probes.

The typical computer oscillograms of the total voltage in the plasma and the voltages at the particular levels can be seen in Fig. 6. In this series of experiments use was made of four discrete values of starting total voltages U_S: 270, 300, 330 and 360 kV. The plasma voltage decreases down in time both on account of the currents through the plasma and an additional low current in the power supply system; the latter is needed to provide a reliable operation of a set of valves-thyristors. Voltage drop at some of the levels, ΔU_N, is intensified during the discharge, this drop at the electrodes near the inner liner being more noticeable since the bulk plasma density is concentrated in this region. The quantity ΔU_N is determined by the discharging the capacitors and also by voltage drops at the ballast resistors (50 Ohm). The energy consumption of the storage unit is 7—20 kJ at a total energy in store of up to 50—100 kJ. Fig. 7 illustrates the voltage distribution on the electrodes at different moments of the discharge. The radial distribution of currents J_N, is given in Fig. 8 at different regimes for $t=200$ μs from the ignition of the discharge.

The $J_N(r)$ curve is of the form qualitatively similar to the distribution of $n(r)$. We observe the region where the longitudinal electron current reduced and coincided with the similar region on the curve for $n(r)$. On the left of this region, the current density increases as the distance from the outer liner increases, while on the right of the local minimum the currents are comparable, unlike the function $n(r)$, with the maximum currents on the left branch of the curve.

The absolute value of the total current flowing to the end electrodes ΣJ_N, lies within 30 to 70 A and is approximately the same as the value of the total ion current flowing to the inner liner I_{23}. The

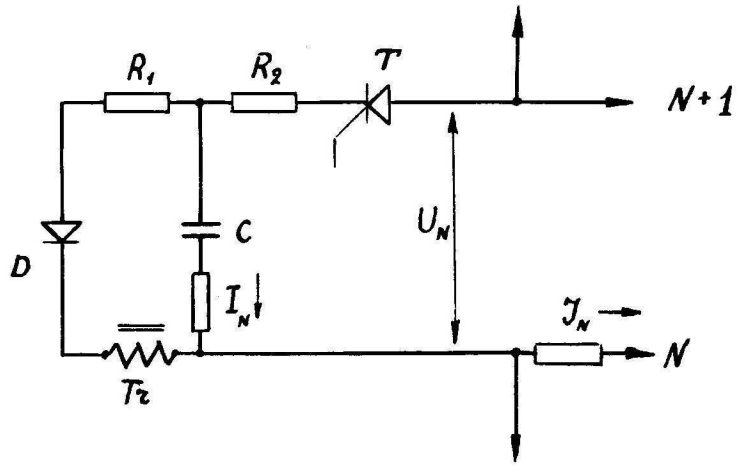

Fig. 5. High-voltage power supply unit of the N-th level and current and voltage control elements.

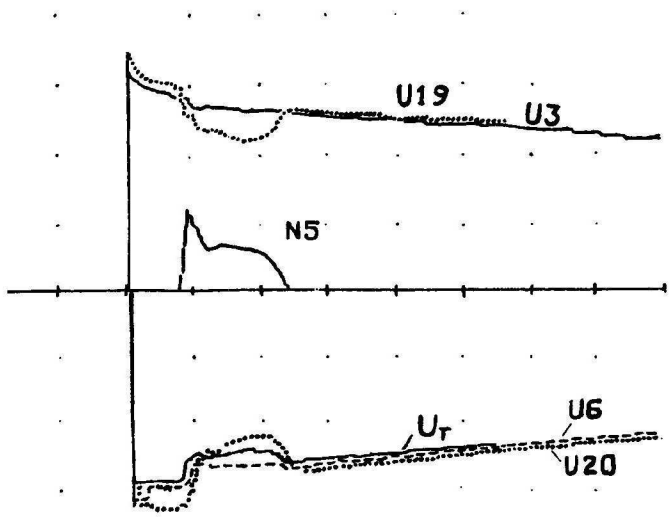

Fig. 6. Typical oscillograms for U_t, U_N, N_5; one scale division in the vertical is 100 kV and in time 0.4 ms.

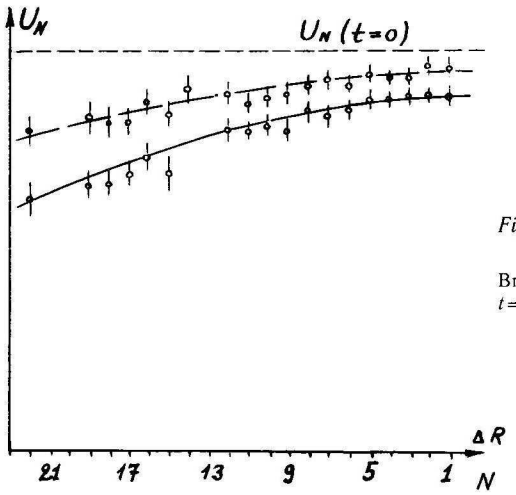

Fig. 7. Radial distribution of the potentials at electrodes U_N:
Broken line: $t=200\,\mu s$ —; solid line: $t=500\,\mu s$; dots mean values of U_N in a 5-shot series.

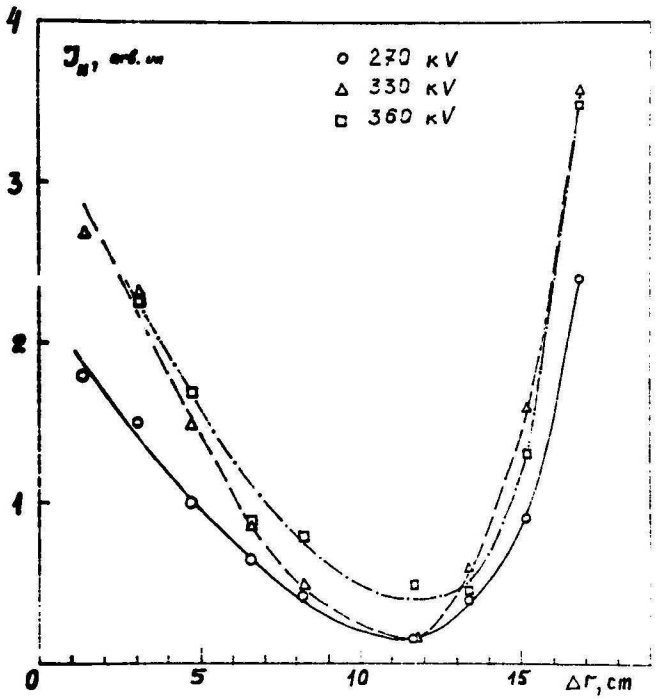

Fig. 8. Radial distribution of J_N.

typical oscillograms of J_N on some of the electrodes are shown in Fig. 9,*a*.

The I_N measurements were used for monitoring the operation of the storage unit in adjustment regimes, and also for J_N control. The typical oscillograms for the current I_N are in Fig. 9,*b*.

The potentials and currents presented above were registered by an «active» electrode system; the information was obtained by means of 1.0 MV optoelectronic systems [11]. A «passive» electrode system is located under the floating potential.

2.3. Neutral Charge Exchange Atoms

1. For direct measurements of the plasma rotation velocity and for measurements of the mean «thermal» ion energy we have studied the spectrum of fast neutral hydrogen atoms formed by plasma ions in the charge exchange process on cold neutral hydrogen atoms (see Fig. 2); the velocity of plasma rotation at different points over the radius was measured by the edge of this spectrum. The radial resolution of an analyser was $+2.5$ mm, and the energy resolution was $+2.5$ kV. The conditions for the shape of $U(r)$ allowing the shape of this function to be reconstructed unambiguously were satisfied in all measurements (see Ref. [12]).

Fig. 10 shows the typical energy spectra of neutral charge exchange atoms. When reconstructing the spectra the detection efficiency has been assumed to be energy-independent since in the energy range under consideration (20 to 60 keV) the efficiency varied by no more than a factor of 1.5—2 on account of both the change of the charge exchange $\langle \sigma v \rangle$ in the plasma and the rate of stripping in the stripping cell. This estimate is consistent with the results of Ref. [13]. This change in the efficiency has no influence on the results when reconstructing the $U(r)$ function.

The shape of the spectra somewhat changes as the total voltage U_S grows: the most noticeable changes were observed in going from 330 to 360 kV.

To compare the energy distributions obtained with the simplest theoretical model the distributions of the neutral charge exchange atoms along the chords were calculated. Into account was taken the real distribution of $n(r)$ and $n_0(r)$; the «thermal» ion energy was assumed to diminish linearly in time from $W=W_E$ to $W_E(1-2\xi)$. For $\xi=0.1\div0.25$ the energy spectra coincide well with the experimental ones. Here the average «thermal» ion energy W_i is about

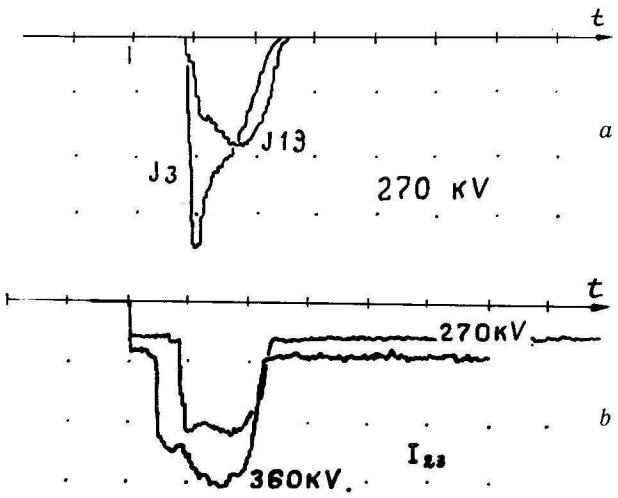

Fig. 9. Oscillograms:
$J_N(t)$ and $I_N(t)$; the time step is 0.4 ms.

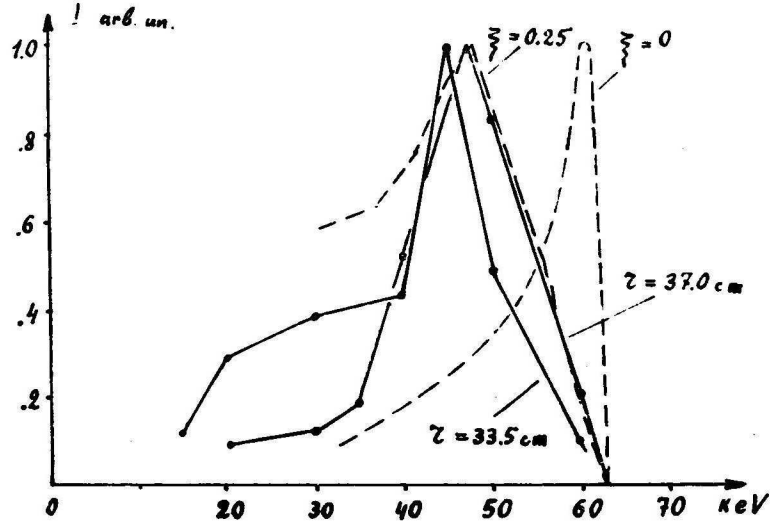

Fig. 10. Energy spectra of neutral charge exchange atoms:
Solid line—experiment, $r=33.5$ and 37 cm ($\Delta r=1.5$ cm; 5.0 cm); broken line—calculation, $r=37$ cm.

$(1-\xi)W_E$ or $0.9\div0.75W_E$. It is obvious that the ions transfer a portion of their thermal energy to the electrons.

2. The flux of fast charge exchange atoms from the plasma was also controlled by detectors for «neutral» fluxes (or secondary emission detectors—SED) (see [6]). Such a detector registers an average flux of fast atoms at an energy more than 1.0 keV. In our experiments, we used five detectors positioned on the outer liner at different distances from the central plane of the trap, the incident ions having been collimated in the z-direction. In detectors, there was compensation of the flux of γ-quanta which are also capable of giving the emission of secondary electrons.

We can reconstruct (fairly roughly) the plasma density distributions along the axis of the device by comparing signals from detectors. Fig. 11 presents the oscillograms from «neutral» detectors lo-

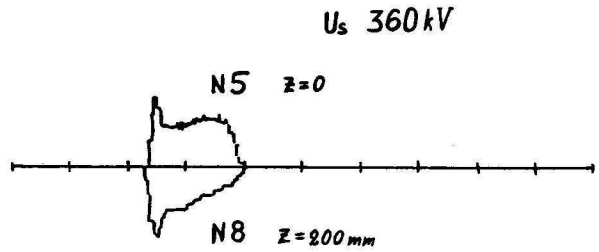

Fig. 11. Signals of «neutral» detectors positioned on $z=0$ and $z=200$ mm (for easiness in interpretation, the signals are of the different polarity).

cated in the central plane and at distance of 20 cm from it. The signal level at detectors near the end electrodes (2 cm from the end electrodes) was considerably lower (lower than 0.1 compared to the signal at the center). So the longitudinal plasma size was of the order of 40 cm.

2.4. H_α Profile

The distribution function of neutral charge exchange atoms with respect to velocities has also studied by broadening the hydrogen line H_α. The experiment was arranged similarly to the previous ones of this series (Ref. [12]). The basic components of the optical system are seen in Fig. 2. The procedure of measurements was based on the Doppler shift in radiation frequency of neutral atoms which are formed in a plasma as a result of the resonance charge

exchange to the excited level with the principal quantum number $q=3$. The H_α radiation spectrum from the local rotating plasma region of radius r, which has been measured along a chord with the impact parameter r_n, has a maximum shift relative to the line λ on $\Delta\lambda$, where

$$\Delta\lambda=\lambda\frac{V_E(r)\,(1+r_n/r)}{c}. \qquad (1)$$

If the condition

$$V_E(r)<\frac{2\,V_E(r_n)}{1+r_n/r} \qquad (2)$$

is fulfilled, the boundary of spectrum, measured along the chord, is determined by the region where the plasma has the least radius r_n. Condition (2) was always satisfied in this experiment. Thus, measuring $\Delta\lambda$ for different impact parameters we can reconstruct the profile $V_E(r)$. It is worth noting that this procedure is inapplicable at high plasma densities because of the fact that the bulk fraction of particles is charge exchanged to the ground state ($q=1$) and can then be excited, in flight, by plasma particles. Estimations, however, show that for our parameters ($n\leqslant 10^{12}\,\mathrm{cm}^{-3}$, $V_E\geqslant 1\cdot 10^8\,\mathrm{cm\cdot s}^{-1}$) such an additional radiation is not large ($\sim 1\%$).

Fig. 12 shows the H_α shapes obtained at $U_S=360$ and 270 kV. In comparison with the experiment described in [12], the spectral intensity of the signal was noticeably weaker and this necessitates a greater number of «shots» to obtain the H_α profiles. For this reason, in this experiment the «hot» spectral components were measured mainly along one chord near the inner liner.

It is worth noting that the values of V_E, obtained by this method, coincide with the appropriate values obtained when processing the charge exchange spectra (see Fig. 13)

With increasing U_S from 270 to 330 kV, a broadening of the H_α line proportional to V_E is observed. When going from 330 to 360 kV the H_α in the stationary part of the discharge changes substantially, and there appears a significant signal in the spectral region corresponding to the motion of charge exchange atoms in the opposite direction.

We also measured the intensity of the «cold» H_α peak ($\lambda=6563$ Å) whose formation is due to the excitation of the atomic neutral gas in the trap volume by plasma particles. Chordic measurements of this signal offer the possibility to reconstruct the local

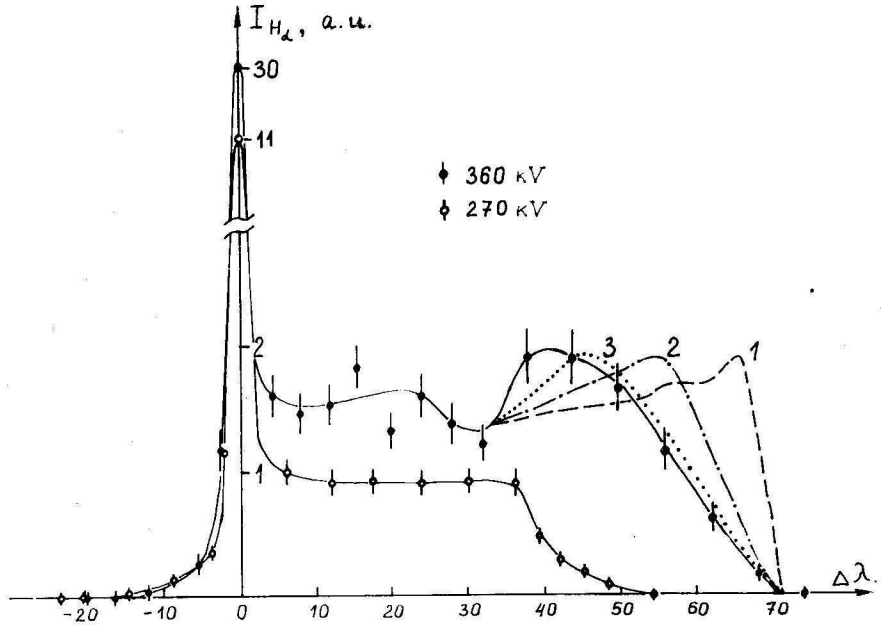

Fig. 12.1. H_α profiles in different regimes. **Experimental dots**: $U_S=270$ kV ($t=100\div 500$ μs), $U_S=360$ kV ($t=100$ μs); **calculated curves** for $U_S=360$ kV ($t=100$ μs): $\xi=0$ (*1*), $\xi=0.15$ (*2*), $\xi=0.3$ (*3*).

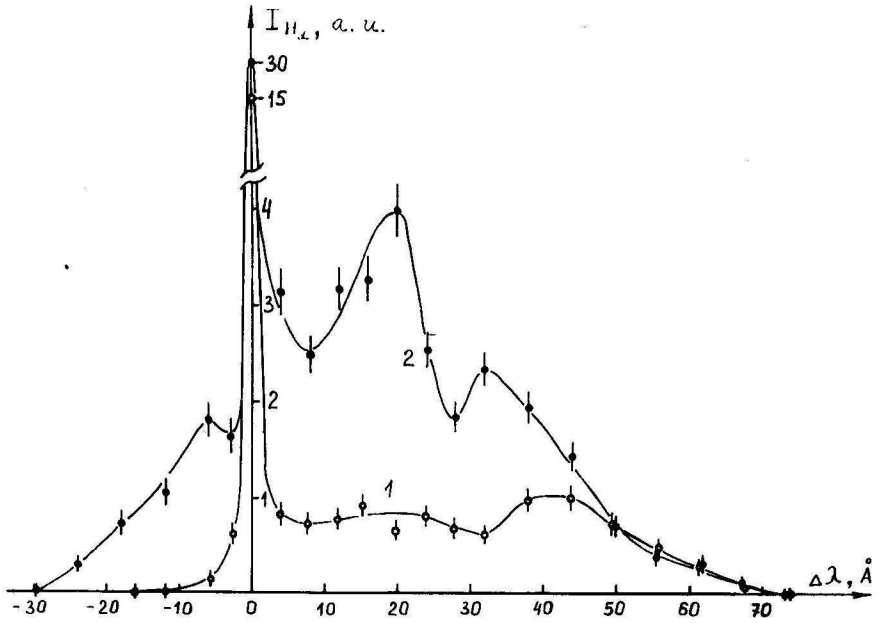

Puc. 12.2. H_α profiles at $U_S = 360$ kV for different moments of time: $t = 100$ μs (*1*), $t = 200 \div 500$ μs (*2*).

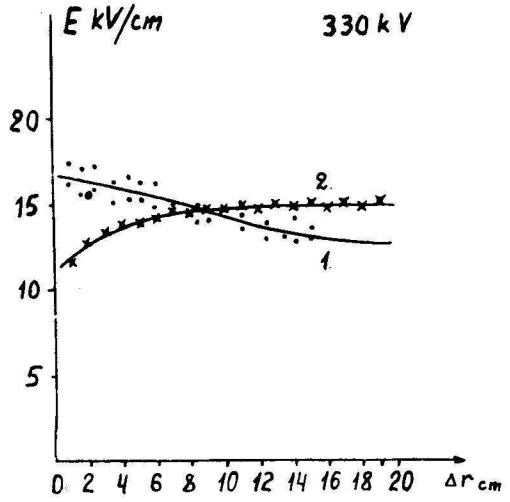

Fig. 13. Distribution of $E(r)$:

1 — with respect to the velocity of plasma rotation, ● — experimental points from the energy spectra for charge exchange neutrals, ⊙ — those from the H_α profile; *2* — projection of the electric field at the end electrodes onto the center of plasma; × — experimental points.

intensity of $n \cdot n_0 \cdot S_{H_\alpha}$; here the method applied is similar to the method for finding the distribution $n(r)$. In a broad range of electron temperatures (50 eV — 10 keV), the rate of excitation of S_{H_α} changes insignificantly. Correspondingly, making allowance for the peculiarities of the plasma under analysis, the quantity S_{H_α} was assumed to be constant when reconstructing the function $n \cdot n_0$ (see Sect. 3.1).

2.5. Potential Distribution in a Plasma

Potentials at the electrodes and potentials in the rotating plasma volume on one and the same magnetic surface should coincide with an accuracy up to $e\Delta\varphi \simeq AT_e$, where $A = 2 \div 5$; in a nonmaxwellian plasma we may take $\bar{W}_e$, instead of T_e [4]. For checking this relation and for reconstructing the function $U(r)$, all the energy spectra obtained were processed. The maximum ion energy on the chord under consideration, which corresponds to a four-fold energy of ion drift on a given radius, is determined by the position of the spectrum edge. Here, for ambiguity of the reconstruction of $U(r)$, an

additional condition for the rate of variation of V_E on the radius

$$V_E(r) < r \frac{\partial V_E(r)}{\partial r} \tag{3}$$

should be fulfilled [12]. Near the positive liner in the $r > r_2 - 2\rho_i$ range, the quantity V_E is reconstructed via extrapolation.

The total plasma voltage, obtained from the measured V_E (or $W_E(r)$), coincides with that obtained from direct measurements U_t with an accuracy of about 5%. The discrepancy between them lies within the accuracy of reconstruction of $V_E(r)$.

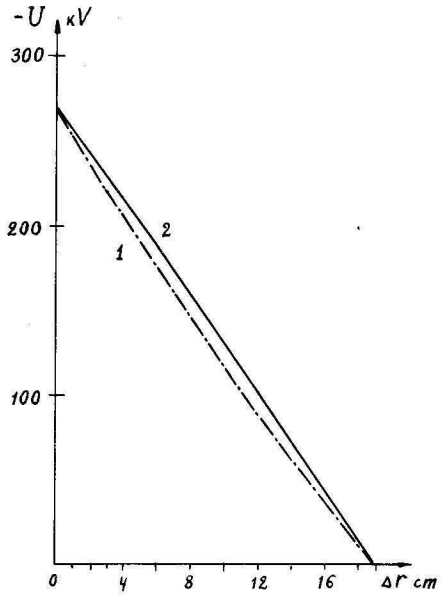

Fig. 14. Potential distribution in the central plane $U(r)$ (*1*), and potential projection at the end electrodes onto the center of the plasma (*2*), U_S=330 kV.

Fig. 13 shows both the magnitude of the electric field on electrodes, projected along the magnetic force lines onto the center of the trap, and the magnitude of $E(r)$, reconstructed from the energy spectra (330 kV). Also given is the value of $E(r)$ at a point, obtained after processing of the H_α profile. **These** data are used to find the potential in the center of the trap (see Fig. 14). In all cases, there exists a 10—30 kV deep potential well for electrons in the center of the trap. The longitudinal energy of electrons leaving the trap may be estimated proceeding from the potential distribution. It is clear that the escaping electrons («tail» of the distribution function) have an energy of up to 30 keV. The whole set of experimental data are in agreement with the assumption that the mean longitudinal electron energy lies within several hundred electronvolts.

2.6. Neutral Gas

When using cryogenic pumping, the pressure of the residual neutral gas was roughly $1 \cdot 10^{-7}$ torr. After a series of shots ($\sim 10^2$), hydrogen was the major component of the residual gas (amount of O_2, N_2 and H_2O was less than 1%).

For the discharge to be formed, we introduced into the chamber a given amount of molecular hydrogen through six electrodynamic valves equally spaced on the azimuth and filled with gas under a pressure of 100—200 torr (valve volume 0.14 cm^3, opening time 0.1 ms). The discharge was ignited approximately 0.5 ms after the valves were opened. By estimation, the amount of the gas flowing to the working volume is 0.3—0.7 of that stored in the gas valves. With the chamber volume (0.6 m^3) and the delay time of discharge ignition taken into consideration, the average density of the atomic neutral gas in the discharge was roughly $1 \cdot 10^{12}$ cm^{-3}. This value may also be derived from the other independent estimation (see Sect. 2.7 and 3.1). The relationship between H and H_2 gas density will be considered in Sect. 3.1.

The presence of heavy impurities in the neutral gas during the discharge was controlled by the intensity of the spectral lines. Their relative content was fairly low: less than $2 \cdot 10^{-4}$ for Fe, Cr and Ni and less than $2 \cdot 10^{-3}$ for Ti. The fraction of heavy ions Ti^+ and Fe^+ in the plasma was about $5 \cdot 10^{-6}$. A considerable reduction of the fraction of heavy impurities, compared with [3], is provided by a protection lattice, composed of Ti rings, on the inner liner.

For monitoring the gas pressure, fast pressure gauges of the Penning-cell type were positioned behind the outer liner. A noticeable increase in the pressure behind the liner was only after the discharge stopped, i. e. gas release under the action of fast neutral atoms and plasma radiation has in practice no effect on the discharge burning regime.

2.7. Ignition and Quenching of Discharge

The discharge was ignited under a gas pressure in the chamber of $5\cdot10^{11}-5\cdot10^{12}\,\mathrm{cm}^{-3}$. A drastic decrease in the pressure (several times lower as compared with the standard) gives no possibility to ignite the discharge: under a pressure higher than $5\cdot10^{12}\,\mathrm{cm}^{-3}$ either breakdowns take place on electrodes since discharge ignition conditions on the left branch of Pachen's curve near electrodes are fulfilled [14], or breakdowns of the S-discharge type occur in the plasma volume because of a reduction of E field near the inner liner (voltage drop on ballasts). For discharge ignition, the distribution of vacuum potentials in the chamber was likely to play a significant role: it created an electrostatic «well» for electrons, with uniform potential distribution on the end electrodes (see Fig. 14). As seen from the radial distributions of currents, the discharge starts to develop near the outer (positive) liner and then extends the whole of the volume over the radius.

Quenching of a discharge occurred 0.5—1.0 ms after the discharge ignition. As have already been mentioned, after the discharge was quenched the electrode voltage became full again, i.e. this event was connected with neither breakdowns nor any change of the electrode voltage. The moment of quenching is explicitly due to a sharp decrease in the degree of ionization in the vicinity of the positive liner, as it is seen from the oscillograms for n (see Fig. 4) and current J_3 at the moment of discharge quenching (see Fig. 9). After that, the front of lowering the plasma density shifts towards the inner liner.

It is more probable that a reduction of n and J_3 near the outer liner is caused either by the disappearance of the electrostatic «well» for electrons in this region (it is impossible to observe the potentials in this region using the above method for measuring $U(r)$), or by changes of the shape of the potential «well», for example, by its narrowing towards the center; the latter also contributes to diminishing the rate of ionization. One more mechanism of reducing n and J_3 is possible: a decrease in density n_0 in the vicinity of the outer liner down to a certain boundary value at which the discharge quenches.

The rate of development and quenching is determined by the «drift» velocity of charge exchange $V_{cx}=\varepsilon/\tau_{cx}$ (for ε see Sect. 3.1): it is the velocity at which the front of discharge moves from the positive to the negative liner for time $(r_2-r_1)/V_{cx}$. The dynamics of

this process is confirmed by a change of the density profile in time (see Fig. 4). The velocity of propagation of the density front corresponds to $V_{cx}=10^5\,\mathrm{cm/s}$. Similar information is given by the time relations between J_N (or U_N) at different levels.

These data enable the density of the neutral gas in the plasma to be estimated: $n_0=V_{cx}/\varepsilon\cdot\langle\sigma v\rangle_{cx}$. For $U_S=360\,\mathrm{kV}$ we get $n_0\simeq1\cdot10^{12}\,\mathrm{cm}^{-3}$.

2.8. Fluxes of Fast Particles to the Trap Walls

Among the factors which limit the plasma density and U_S we may call the fluxes of fast particles—neutral charge exchange atoms—to the wall and end electrodes. When this parameter exceeds some limiting value there have been breakdowns in the plasma, with a very smooth front of current increase: $10^{-5}-10^{-4}\,\mathrm{s}$. The mechanism of developing this process is assumed to be as follows: the reverse hydrogen flow increases; this leads to an avalanche-like increase in the density of neutral atom in the plasma and, as a consequence, to the fulfillment of the conditions for a breakdown according to the left branch of the Paschen's curve [14] or to the S-discharge.

The average fluxes of fast particles to the walls ($\bar{p}$) may be estimated from the relation

$$\bar{p}\simeq n\,V/\tau_{cx}\cdot S\,, \tag{4}$$

where V is the plasma volume and S is the wall surface.

For the typical parameters of experiment: plasma density $n=3\cdot10^{11}\,\mathrm{cm}^{-3}$, charge exchange time $\tau_{cx}=10^{-5}\,\mathrm{s}$, $V=0.5\cdot10^5\,\mathrm{cm}^3$ and $S=10^5\,\mathrm{cm}^2$, we obtaine the particle flux roughly equal to $1.5\cdot10^{16}\,\mathrm{cm}^{-2}\cdot\mathrm{s}^{-1}$ for energy of particles $0<W<8\cdot10^4\,\mathrm{eV}$. This corresponds to an energy flux higher than $100\,\mathrm{W/cm}^2$ in fast particles. This estimate only deals with the average fluxes and one may assume that the flux to the end electrodes is about 10 to 20 $\mathrm{W/cm}^2$ because of multiple reflections from the wall.

These fluxes are comparable with those to the walls in full-scale thermonuclear devices. At typical parameters ($n=10^{14}\,\mathrm{cm}^{-3}$, $\tau=3\,\mathrm{s}$ and $V/S=10\div100\,\mathrm{cm}$) we obtain from eq. (4) the quantity $\bar{p}$ one order of magnitude less as compared with the above estimates. A comparison of these fluxes is rather approximate (the difference in angular distributions and in the composition of fast particles, as

well as the stationary and pulse systems), but it is, however, evident that a high-voltage system generating radial electric fields in a plasma may also operate in the regime of real thermonuclear parameters.

3. DISCUSSION

3.1. Properties of the E×B Discharge

A. We will treat the properties of the $E \times B$-discharge in a magnetic trap provided that Coulomb scattering proceeds considerably slower than ionization and charge exchange. The continuity equation describing the processes in the stationary discharge is of the form

$$\partial n/\partial t = -\operatorname{div}(n \cdot \vec{v}_{cx}), \tag{5}$$

where $\partial n/\partial t = n \cdot n_0 \langle \sigma v \rangle_i$ is the ionization rate at point r; note that this equation incorporates ionization by ions and electrons.

If the plasma is in axisymmetrical trap and the ion component of the plasma has no z-average velocity, eq. (5) may be considered as one-dimensional, and then $\operatorname{div}(n v_{cx}) = \frac{1}{r} \cdot \frac{\partial}{\partial r} (r n n_0 \langle \sigma v \cdot \delta r \rangle_{cx})$ is the term related to charge exchange, $n_0 \langle \sigma v \cdot \delta r \rangle_{cx} = V_{cx}$ is the «velocity» of the charge exchange drift, δr is the radial shift of the center of the Larmor orbit in every step of charge exchange. We may write $\langle \sigma v \cdot \delta r \rangle_{cx} \equiv \langle \sigma v \rangle_{cx} \cdot \langle \delta r \rangle$, where $\langle \delta r \rangle \equiv \varepsilon$ is the average shift of the center of the Larmor orbit during the period of charge exchange.

In the above expressions, averaging takes account of the real conditions of ion motion in crossed fields.

Assuming that at the point r_0 (for instance, near the positive liner) the plasma density is fixed in any way, it is found to obey the law

$$n(r) = n(r_0) \frac{n_0(r_0)\, r_0}{n_0(r)\, r} \exp(r_0 - r)/\chi_0, \tag{6}$$

where $\chi_0 = \langle \sigma v \delta r \rangle_{cx} / \langle \sigma v \rangle_i$ (see Fig. 17). For a given value of T_e, the quantity χ_0/ρ_i is a function of only one parameter, V_E, or for fixed a/ρ_i and $V_E(r) = \text{const}$ a function U_T.

The basic parameters of the plasma, r-dependent and controllable in experiments, can be expressed using eq. (6). The density of the longitudinal electron current $j_\parallel = J_N / 2\pi r_N \cdot \Delta r_N$ may be represented either as

$$j_\parallel(r) = e \int_{-z}^{z} n_0 n \langle \sigma v \rangle_i dz \sim L(z)\, n_0 n \langle \sigma v \rangle_i \tag{7}$$

or under the assumption that the plasma dimension $L(z)$ and the ionization rate are independent of the radius

$$j_\parallel(r) \sim n_0 \cdot n, \tag{7'}$$

where $n_0 \cdot n$ vary, over the radius, according to eq. (6).

The flux of neutral charge exchange atoms at the top edge of the energy spectrum p_{cx} along the chord with impact parameter r is as follows

$$p_{cx}(r) = n n_0 \langle \sigma v \rangle_{cx} \int^{\Delta x} \int^{\Delta\Omega} f_i(v_\parallel, v_\perp, x)\, d\Omega\, dx, \tag{8}$$

where $\Delta\Omega$ is the solid angle in the velocity space of charge exchange neutrals, which is determined by a collimator of the energy analyzer; x is the coordinate along the observation chord; Δx is determined by the analyzer energy «window». If the function f_i is independent of (or weakly dependent on) r, and $V_E(r) = \text{const}$, i. e. $\langle \sigma v \rangle_{cx} = \text{const}$, then $p_{cx}(r) \sim n_0 n r$.

If there is a noticeable radial plasma diffusion caused by oscillations, the diffusion term should be introduced into eq. (5)

$$n n_0 \langle \sigma v \rangle_i = \frac{1}{r} \frac{\partial}{\partial r} (r n n_0 \langle \sigma v\, \delta r \rangle_{cx}) + \frac{1}{r} \frac{\partial}{\partial r} \left(r D \frac{\partial n}{\partial r} \right). \tag{9}$$

With n и D assumed to be invariable over the radius, the solution of (9) is of the form

$$n n_0 r = n n_0 r|_{r=r_0} \cdot \exp(r_0 - r)/\chi,$$

where

$$\chi = (\chi_0/2)\,(1 + (1 + 4D/\chi_0 \cdot v_{cx})^{1/2}). \tag{10}$$

It the case when the quantity χ is known from experiment, we may define

$$D = \chi(\chi/\chi_0 - 1) \cdot v_{cx}. \tag{11}$$

B. We will compare the theoretical and experimental radial distribution curves of the basic plasma parameters in the stationary phase of discharge.

We reconstruct the function $n_0(r)$ from the experimental diagrams for $I_{H_\alpha}(r)$ for the cold component and the from the function $n(r)$ obtained from the interferometric measurements (see Figs 15.1 and 15.2).

A simular result can be derived from the shape of the spectra for charge exchange neutrals; the local values of the function $n_0 n$ are found proceeding from the signal intensity p_{cx} at the top edge of charge exchange spectrum; this intensity is determined by the flux of particles from the region where the impact parameter is minimal.

The experimental radial distributions of the plasma density and the theoretical $n(r)$ curves obtained from (6) and (10) under different assumptions for $n_0(r)$ and D are also shown in these figures. At $U_S = 270$, 300 and 330 kV the discrepancy between the theoretical and experimental curves lies within measurement errors, while at $U_S = 360$ kV these are very substantial.

Variation of the neutral density near the inner liner with time and $n(t)$ are presented in Fig. 3; it is seen from these function that the radial increase in the plasma density is limited because of the increase in n_0. These increased densities of the neutral gas in the vicinity of the inner liner are due to desorption and remission of the atomic hydrogen which are caused by the flux of fast charge exchange atoms arrived at this liner. About half of all the fast atoms from the plasma are incident on it. The central section of the outher liner was made from thin rings and, therefore, was transparent for these atoms. Thus, the density profile of the neutral gas is formed in the plasma which increases to the inner liner and limits the growth of $n(r)$ (see. eq. (6)). It is clear that the profile $n_0(r)$ should be consistent with the density distribution of the plasma. When checking this, the velocity distribution function of secondary neutral atoms is an unknown parameter. Good agreement of the experimental and theoretical dependences is obtained (see Figs 15.1, 15.2) under the assumption that the bulk of hydrogen atoms leaving the inner liner corresponds to Tompson's energy distribution [15]. In this case, if we put for the surface binding energy of the Tompson distribution $E_b = 1.3$ eV, which has been measured in [16], besides fast atoms a small amount (about 8%) of the cold ($T \sim 300$ K) gas flow is required. A number of experimental data: the absence of charge exchange molecules (coincidence of the maxi-

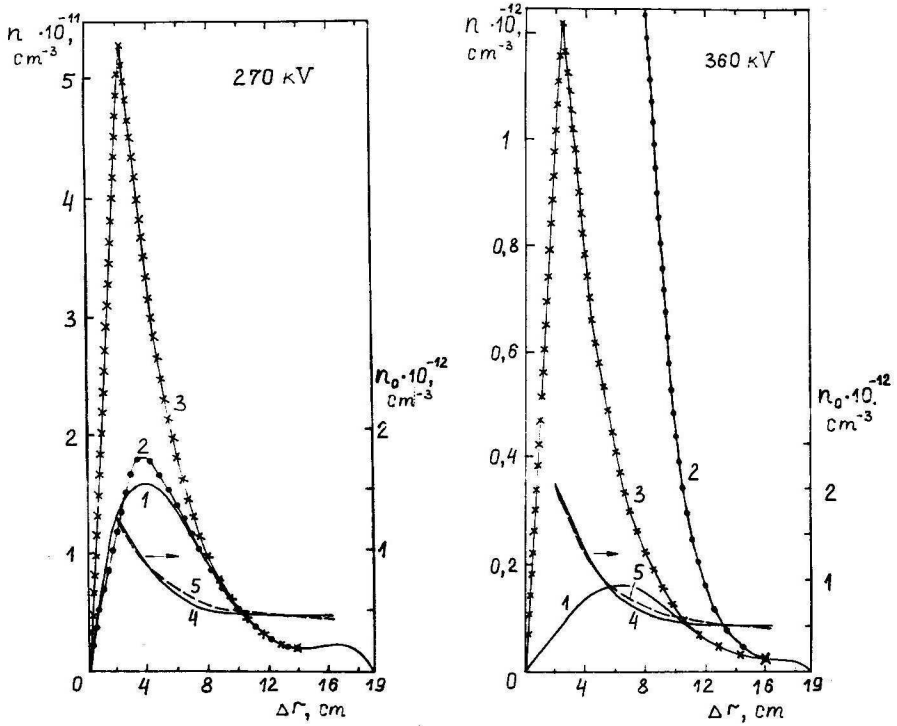

Fig. 15.1. Radial profiles of the plasma and neutral-gas densities at $U_S = 270$ kV. $h(r)$ plasma density: *1*—experiment ($t = 200$ μs); *2*—calculation at $D = 0$, $n_0(r)$—experimental data; *3*—calculation at $D = 0$, $n_0(r) = \text{const}$; $n_0(r)$—**neutral gas density**: *4*—experiment; *5*—calculation.

Fig. 15.2. Radial profiles of the plasma and neutral-gas densities at $U_S = 360$ kV. $n(r)$—**plasma density**: *1*—experiment ($t = 200$ μs); *2*—calculation at $D = 0$; $n_0(r)$—experimental data; *3*—calculation at $D = 10^6$ cm$^2 \cdot$ c^{-1}, $n_0(r) = \text{const}$; $n_0(r)$—**neutral gas density**: *4*—experiment; *5*—calculation.

mum boundary energies measured on the H_α line and also the data of an analyzer of charge exchange neutrals; concidence of U_T obtained from the data of charge exchange neutrals analyzer and direct measurements) the absence of molecular ions (falling off the density near the inner liner at a distance appoximately equal to two Larmor radii for H^+) evidence that the plasma volume is mainly filled with the atomic hydrogen. The relatively small fraction of the molecular hydrogen is accounted for by the fact that the flow of atomic hydrogen from the titanium wall, which is caused by its bombardment of neutral charge exchange atoms and ions can be much more intense than the flow of molecules leaving the surface because of thermal desorption. The molecular hydrogen, filled through the valves, charge exchanges in volume and dissociates on the wall for 50 μs after the discharge onset.

The shape of the function $j_\parallel(r)$ is described in detail in Sect. 2.2. Near the outer liner we have observed the currents comparable with the maximum ones. Here $j_\parallel(r)$ is greatly different from the $n(r)$ diagram. The effect is explained by the fact that on a size, roughly equal to two or three ion Larmor radii (near the positive liner) the discharge is initiated mainly due to longitudinal electric fields and determined by electron ionization. As seen from the comparison of the current and plasma density measurements, this discharge occupies the region along the z-axis from mirror to mirror. In the charge exchange process, the ions leave this, over r, for the more «shallow» potential longitudinal well region (higher electric potentials pulling ions the trap), and therefore, some portion of these ions on the $r=r^*$ area can go to the end electrodes. The reduction of $j_\parallel(r)$ near the point r^* is most likely to be caused by this process. On the left of this point, there has been observed an exponential increase in current density. Comparison of the $j_\parallel(r)$ and nn_0 curves in this region shows that the factor $L(z)$ in (7) is nearly independent of the radius (see Fig. 16). This makes it possible to use the one-dimensional discontinuity equation in the description of the plasma, as it has been made above.

Fig. 16 illustrates the shapes of the functions discussed above in logarithmic scale, as well as the shapes of the theoretical curves at different U_S.

The function $\chi(V_E)$, calculated by (6) for $\xi=0.25$ and $\langle\sigma v\rangle_i^e = 2.7\cdot10^{-8}\text{cm}^3\cdot\text{s}^{-1}$, and the experimental values of χ, for different V_E, which were obtained from the data in Fig. 16, are shown in Fig. 17.

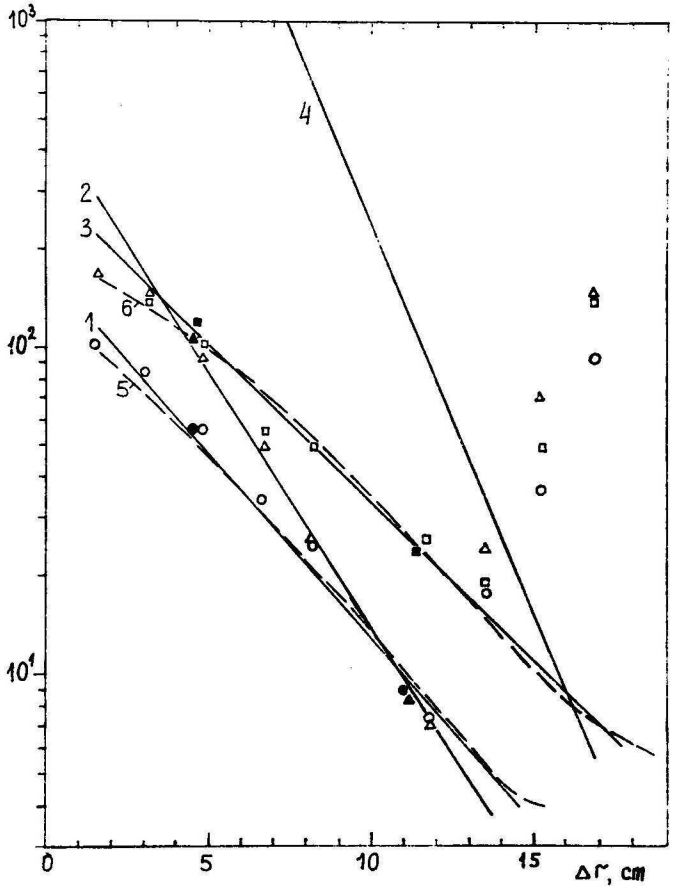

Fig. 16. Radial distributions of the functions (in relative units): ○, △, □ — $J_N \sim nn_0 r$; ●, ▲, ■ — $p_{cx}(r) \sim nn_0(r)$; broken line — $I_{H_\alpha}\cdot r \sim nn_0 r$ from the H_α «cold peak» measurements; solid lines (*1*, *2*, *3*) — averaged shape of the function $nn_0 r$ (experiment); regimes: $U_S = 270$ kV (○, ●) — curves *1* and *5*; $U_S = 330$ kV (△, ▲ — curve *2*; $U_S = 360$ kV (□, ■) — *3* and *6*; calculation for $U_S = 360$ kV at $D=0$ — curve *4*.

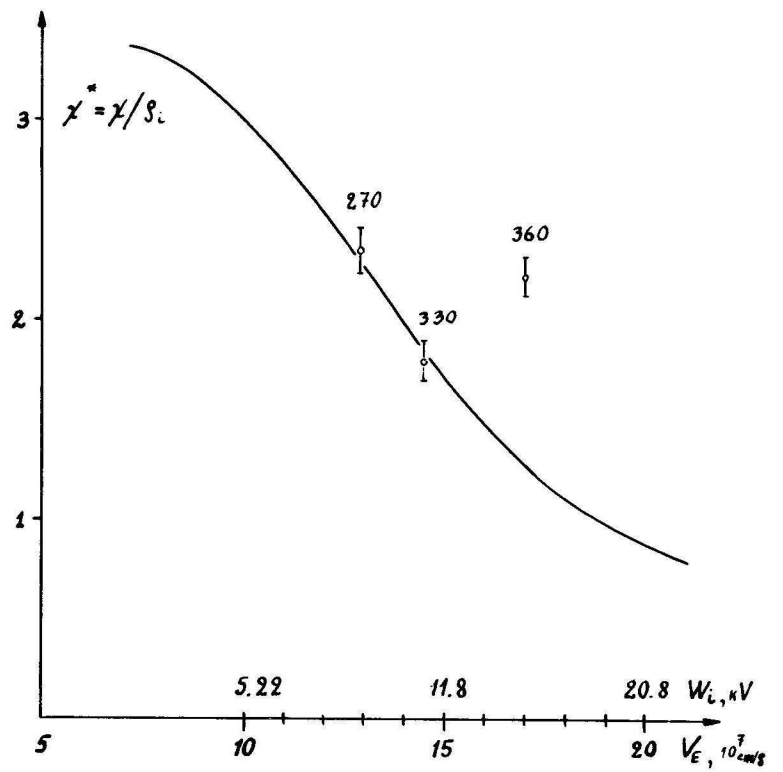

Fig. 17. Function $\chi(V_E)$: solid line—calculation, $\langle \sigma v \rangle_i^e = 2.7 \cdot 10^{-8}$ cm$^3 \cdot$s^{-1}, $\xi = 0.25$; Φ—experimental points for $U_S = 270$, 330 and 360 kV.

Comparison of the above curves with the theoretical classical calculations demonstrates a consistence between them within measurement errors in the $U_S = 270 \div 330$ kV regimes, i. e. there is no radial diffusion of both the ions and the electrons.

The maximum D, which has been obtained under the assumption that a possible discrepancy between the experimental and the theoretical values of parameter χ (equal to the measurement error) caused by radial diffusion, amounts to $4 \cdot 10^4$ cm$^2 \cdot$s^{-1}, the appropriate calculated time of radial losses is $\tau_D > 2 \cdot 10^{-3}$ s. For $U_S = 360$ kV the shapes of the curves show that an intense radial transfer occurs in the plasma: χ becomes twice as much as χ_0, and $D = 10^6$ cm$^2 \cdot$s^{-1}, i. e. $\tau_D = 10^{-4}$ s is comparable with the characteristic lifetime of the particles in the plasma.

3.2. Plasma Instabilities

The level of oscillations in the plasma volume was not measured directly. Using near-wall probes, we have fixed a wide spectrum of electrostatic oscillations within the megahertz range at the edge of plasma, the level of which does not vary considerably in the discharge process and when changing the discharge regime. A number of macroscopic effects, observed in the experiment, shows that there exist at least two types of instabilities in this discharge.

The change of discharge regime in going from $U_S = 270 \div 330$ kV to $U_S = 360$ kV, may be accounted for by the appearance of the flute rotational instability. With increasing U_S, the instability increment grows, and the charge exchange cross section reduces, thereby causing a decrease in longitudinal electron currents, the latter being a stabilizer for this instability. At $U_S = 270 \div 330$ kV the theoretical and experimental values of the exponential factor coincide within the experimental error, and we are able to obtain only the estimate for τ_D, $\tau_D > 2 \cdot 10^{-3}$ s (see Fig. 17).

It is worth mentioning that good consistence of the theoretical and experimental values of the exponent factor χ is observed under the condition that electron ionization contributes much enough: $\langle \sigma_e v_e \rangle_i^e = 2.7 \cdot 10^{-8}cm^3 \cdot$s^{-1} or $T_e > 50$ eV; the upper limit of T_e is somewhat obscured here because the quantity $\langle \sigma v \rangle_i^e$ varies weakly when ranging T_e from 50 eV to 1.0 keV.

At $U_S = 360$ kV the quantity τ_D roughly amounts to, in the order of magnitude, the ion life time: 10^{-4} s. In this regime, the shape of the $n(r)$ curve changes to a great extent: it approaches the parabolic distribution. Simultaneously, in the spectrum of the H_α lines the excited atoms moving in the direction opposite to that of plasma rotation are observed (see Fig. 12). This effect is accounted for by a diffusive adiabatic moving of the plasma ions inside the region of the liner slits for τ ($\tau_{cx} \geqslant \tau \gg \omega_c^{-1}$): in this case, the cyclotron rotation of ions continues, and the azimuthal drift rate falls off to zero. Estimation of the radial diffusion coefficient near the inner liner yields for this process

$$D \simeq 2\rho_i^2/\tau_{cx}|_{r=r_1} \approx 10^6 \text{ cm}^2 \cdot \text{s}^{-1}.$$

Thus, in going from $U_S = 330$ kV to $U_S = 360$ kV the MHD instability accompanied by a considerable increase of the radial diffusion is developed.

We will compare the conditions under which the transition to the stable regime occurs with the stabilization criterion previously created by Bekhtenev and Volosov (Ref. [7]). For stabilization, two conditions should be fulfilled. First, the time required for leaving the electrons in the longitudinal direction, τ_e should be less that the characteristic time required for the development of the instability, $\tau_\gamma = \gamma^{-1}$, multiplied by the factor roughly equal to $(\lambda/\rho_i^*)^2$:

$$\tau_\gamma > \tau_e (k\rho_i^*)^2 \approx \tau_e (\rho_i/\lambda)^2 (T_{eef}/T_i) . \qquad (12)$$

Second, the rate of relative slipping of plasma layers should be sufficiently high to stabilize the higher oscillation modes

$$m(\partial \Omega_E / \partial r) \cdot a_n/\pi > \gamma . \qquad (13)$$

Here $\gamma^{-1} \simeq 2 \cdot 10^{-7}$ s,

$$\tau_e (\rho_i/\lambda)^2 \cong \tau_{cx} (a_n/\rho_i)(\rho_i/\lambda)^2 = \tau_{cx}(\rho_i/\lambda) ,$$

here λ is the characteristic wavelength; if, according to [7], we assume $\lambda \simeq a_n$, where a_n is the gradient size of the plasma, then $\rho/\lambda = 1/3$ for the regimes we have studied experimentally.

The quantity T_{eef}, defined as the characteristic energy acquired by the leaving electrons for the last flight between mirrors, can be estimated from the magnitude of the potential barrier for electrons $U \simeq 10 \div 30$ kV and the number (N) of longitudinal oscillations of the electron for the lifetime in the trap. The ratio of the lifetime in the trap ($3 \cdot 10^{-5} \div 10^{-4}$ s) to the flight time at a maximum energy ($\sim 10^{-8}$ s) of about 10^3; therefore, $T_{eef} = e\Delta U / N^{1/2} \simeq 1$ keV. Substituting the above parameters of the plasma into (12), we obtain the equality in the vicinity of $U_S \simeq 330$ kV. On the other hand, the condition (13) also is undoubtedly fulfilled since Ω_E drops over the radius by a factor of 1.5 to 2 because of r and $E(r)$ (see Fig. 13). Thus in the vicinity of $U_S = 330$ kV there must be the boundary of the centrifugal instability, and this is confirmed experimentally (see Fig. 17). At $U_S > 330$ kV the so-called «marginal stability» is observed at which the instability increment is very small, but however sufficient to change the density profile in a way such that the condition (12) continues to be fulfilled (γ increases because of the growth of V_E, while τ_e (and τ_{cx}) increases because of the decrease of σ_{cx} and a_n because of the diffusion). Note that the increment time required for the centrifugal instability to develop about $2 \cdot 10^{-7}$ s, and the characteristic time, determined by the diffusion, is $10^{-3} - 10^{-4}$ s.

It is clear that stabilization here occurs both due to the longitudinal flow of electrons to the end electrodes together with the «electric shear». All the other possible stabilization mechanisms, for example «min B» and density profile stabilization, are destabilizing for this case.

When creating full-scale thermonuclear devices the particle confined time in the trap can be increased up to 1 s, with the stability conserved owing to some factors: an increase of U_S up to 5—10 MV ($U_S/W_i \simeq a/\rho_i$), increase of r by a factor of 5—10 ($\gamma \cong V_E/r$), and a decrease of T_{eef}/T_i due to growth of T_i. This question has been considered in Ref. [7].

In addition to MHD-instabilities, kinetic instabilities associated with a strong nonequilibrium nature of the velocity distribution function of ions are also present in the plasma. For the time of one charge exchange, (10^{-5} s) the ions succeed in changing substantially the initial shape of the distribution function; it is seen from the comparison of the theoretically calculated energy spectrum of the ions (by $\xi = 0$) and the real one (see. Fig. 11), as well as from the shape of the H_α profile (see. Fig. 12).

This instability is most likely to give rise to heating the electrons leaving the trap for the end electrodes. Their energy ranges from 10 to 30 keV, and coincides, in the order of magnitude with the mean energy lost by ions for τ_e.

The kinetic instability, responsible for energy transfer from ions to electrons, is not so significant as the centrifugal instability considered above. In thermonuclear regimes, the bulk of ion energy is assumed to be transferred to the electrons due to Coulomb collisions. Thus this process should be taken into account only in cases of special regimes where $T_e \neq T_i$; on the other hand, at a sufficiently spreaded distribution function, for example, with increasing τ_{cx}, this instability can be absent.

3.3. Limitation of Plasma Density

As has been shown above, the plasma density did not exceed $3 \cdot 10^{11}$ cm^{-3} (10^{12} cm^{-3}). Density limitations with increasing U_S were first and foremost due to a simultaneous increase in the density of the neutral gas on account of the flux of cold neutral atoms knocked out from the inner liner by the flux of fast charge exchange neutrals.

In each act of charge exchange, the ion shifts over the radius by $\langle \delta r \rangle = \varepsilon$; here the fast atom, leaving for the inner liner with a probability of ~0.5 is produced. For the period of time between the ion production due to the ionization and the incidence on the inner liner the ion is subjected to a_n/ε acts of charge exchange (i. e. $a_n/2\varepsilon$ fast atoms fall at each ion incident on the inner liner). The flux of neutral atoms at the inner liner, therefore, is a factor of $a_n/2\varepsilon$ larger than the flux of incident ions. If the inner liner is made transparent for fast atoms, the density of the neutral gas near it will become at least $a_n/2\varepsilon$ times less; however, the flux of ions at the liner remains the same. If the liner is completely removed and the potential is sustained in the center only due to the electron conduction, the density of the neutral gas near the inner boundary of the plasma can be reduced to a more considerable value. In practice, the appearance of the «secondary» neutral atoms in this region can be avoided completely, and the limitations of the plasma density, because n_0 can be eliminated. In this case, the discharge ignition and burning conditions, as well as plasma stabilization conditions can, however, change.

Another limitation on the plasma density is connected with the condition (12). If the increase in density is determined by the decrease in n_0, this will give rise to increasing $\tau_e \sim \tau_{cx}$ and, correspondingly, to violating the condition (12), and, as a consequence, to the lack of stability. This condition can be fulfilled, if the quantity $T_{e.ef}$ reduces with a simultaneous increase of τ_{cx} (we hope to have it due to a certain shortening of the length of the device and a reduction of the mirror ratio).

3.4. Total Voltage

Obtaining high enough radial voltages in the plasma (of the order of megavolts) has been one of the major problems whose solution has made it possible to perform the plasma experiments described above. The HV technology realized at PSP-2, will be described elsewhere; we will here only mention the main peculiarities and some significant results.

Radial electric fields are introduced into a plasma using a sectionalized electrode system (Refs [1—3]). Each pair of electrode is powered independently, and thus any of the sections has no influence on the other at any breakdowns inside the section. In most cases, the breakdown of a particular section does not cause the

breakdown of the system as a whole. As for the total voltage, the breakdown can occur only in the region with high magnetic field and sufficiently high drift velocity ($\sim 2 \cdot 10^8$ cm/s). In view of this, the energy released during the breakdown, is distributed throughout a large enough surface of the electrodes and walls (several orders of magnitude higher that in a usual breakdown). During some of the total breakdowns the energy stored in capacitors achieved 30—100 kJ, after 2-3 conditioning shots at decreased voltage the parameters of the HV section having been restored completely.

A preliminary conditioning of ring electrodes is an obligatory technological procedure for the HV system. To attain the maximum U_S, electrodes were conditioned in pairs (no more than 1 mA current) about 10 hours. Since the radial distribution of the potential was linear, $U_S = NU_{N\min}$, where $U_{N\min}$ is the voltage at a pair of electrodes with minimal U_N. We have to emphasize that after conditioning the pair of electrodes conserves the acquired resulted properties for a long time (U_N drops by several percent for one year).

As has been mentioned above, the inner liner has a special lattice surface, and this enabled the appearance of the *S*-discharge to be suppressed (the discharge with active self-sputtering of the liner wall which creates a plasma with high content of the metal ions) (see Ref. [3]).

There are some other factors which are very important when achieving high voltage at the device: vacuum conditions in the experiment and conditioning (10^{-7} and 10^{-6} torr, respectively), the material of the liner walls and electrodes (Ti and stainless steel), the form of the potential distribution at the end electrodes, etc.

The major result of the experiments under discussion is a confirmation of one of the main ideas of the authors: a practically linear increase of U_S is possible with increasing the number of electrodes in the rotating-plasma trap. The difference from the linear low is explained by the fact that in multi-element systems conditioning takes a prolonged period of time (because of both the number of elements and the total surface area increase), and therefore the somewhat lower voltages are applied to the pairs.

The methods described above have made it possible to obtain the total potentials U_S in the conditioning process: 0.5 MV (24 electrodes, liner-to-liner distance near the electrodes is 11.5 cm) and 0.40 to 0.45 MV in the case of a work with the plasma. No basic limitations on the growth of U_S with the number of electrodes in the conditioning regime have been revealed.

4. CONCLUSION

1. A hot rotating plasma with a mean energy of ions up to 20 keV (in the rotating frame of reference) and electron energy of about 0.1—1.0 keV (nonmaxwellian spectrum) with the upper boundary $W_e = 10 \div 30$ keV has been obtained.

2. A plasma density of up to $3 \cdot 10^{11}$ cm^{-3} has been obtained in most of the operating modes and up to 10^{12} cm^{-3} in special regimes. The limitation of density by rising U_S is caused by two factors: the violation of the MHD stability condition and the increase in the neutral gas density near th inner liner.

3. The existence of the regimes has been shown in which the hot rotating plasma is MHD-stable with a characteristic time of diffusion transverse losses larger that $2 \cdot 10^{-3}$ s ($U_S = 330$ kV). As U_S increases, the plasma transforms into the state of MHD marginal stability with a characteristic diffusion times of about 10^{-4} s. The position of the stability boundary is consistent with the theoretical estimation.

4. An accelerated (as compared to the Coulomb process) loss of the «thermal» energy of ions coupled with the increase of the longitudinal electron energy (up to 10—30 keV), has been observed; this may be explained by the development of the kinetic instability. The explanation of this process by Galeev and Sagdeev seems us the most probable (see Ref. [17]). The instability of this kind must not manifest itself in full-scale PSP-2 based devices.

5. The possibility of the existence of a high-temperature ($W_i = 20$ keV) discharge in crossed $E \times B$ fields without any plasma sources and special heating systems has been shown. There is a good agreement between the observed properties of the discharge and the elementary theory of discharge.

6. The velocities of electric drift (V_E) have been obtained which are much higher than Alfven's critical velocity (V_c). In our case, V_E achieved $2 \cdot 10^8$ cm/s, i. e. it is 40 times larger than V_c ($V_c = 5 \cdot 10^6$ cm/s). No basic limitations on further increase of V_E have been observed. This result evidences that the authors' ideas about the factors hampering the increase of V_E in a rotating plasma and about the methods eliminating these factors are valid.

In the number of the earlier experiments a quasi-stationary plasma with $V_E > V_c$ (by a factor of 3—5) was observed, however the attempt to further increase V_E was not successful. For this reason,

the question dealing with the possibility of plasma production at thermonuclear ion energies ($W_i = 10^4 \div 3 \cdot 10^4$ eV) on the basis of an $E \times B$ trap has remained still open. The results obtained unambiguously speak for such a possibility.

7. It has been shown that being applied to the rotating plasma the total voltage can achieve 0.4—0.5 MV in the quasi-stationary regime. The derived value of U_S lies relatively close to the total voltages necessary for subthermonuclear devices besed on this principle (Refs [1, 18]). These results have been obtained at the fluxes of fast neutral atoms at both the walls and the high-voltage elements, which were close to those expected in the future devices with thermonuclear parameters.

Acknowledgements.

The authors are very grateful to A.A. Bekhtenev for useful discussions; authors would like to thank A.G. Kolachev, K.K. Schreiner, V.Kh. Lev, V.V. Mishagin and R.S. Pritchin for their technical and engineering assistance.

REFERENCES

1. *Bekhtenev A.A., Volosov V.I., Pal'chikov V.E. et al.* Nucl. Fusion, 1980, v.20, p.579.
2. *Abdrashitov G.F., Bekhtenev A.A., Kubarev V.V. et al.* Proc. of the 1983 Varenna School on Plasma Physics, 1983, v.1, p.335.
3. *Volosov V.I., Abdrashitov G.F., Bekhtenev A.A. et al.,* Journal of Nucl. Mat., 1984, v.128-129, p.445.
4. *Lehnert B.* Nucl. Fusion, 1971, v.11, p.485.
5. *Bocharov V.N., Zavadskij N.A., Kiselev A.V. et al.* Pis'ma v JETF, 1985, v.41, p.494.
6. *Abdrashitov G.F., Bajborodin S.I., Bekhtenev A.A. et al.* In: Plasma Physics and Controlled Nucl. Fus. Research (Proc. 8th Int. Conf. Brussels, 1980), IAEA, Vienna, 1981, v.1, p.539.
7. *Bekhtenev A.A., Volosov V.I.* Zh. Tekh. Fiz., 1977, v.47, p.1450.
8. *Bekhtenev A.A., Vandegrift G.G., Volosov V.I.* Fizika Plazmy, 1988, v.14, p.292.
9. *Beloborodov A.V., Kubarev V.V., Mishagin V.V.* Diagnostika Plazmy, v.6. M.: Energoatomizdat, 1988, p.137.
   Kubarev V.V., Mishagin V.V. Preprint INP 86-45. Novosibirsk, 1986.
10. *Beloborodov A.V., Kubarev V.V.* Preprint INP 88-144. Novosibirsk, 1988.
11. *Bajborodin S.I., Belkin V.S.* Proc. of Allunion school-conf. «Sovremennye metody magnitnogo uderjanija, nagreva i diagnostiki plazmy». Vol.2. Khar'kov, 1982, p.81.
12. *Abdrashitov G.F., Bajborodin S.I., Bekhtenev A.A. et al.* Voprosy Atomnoy Nauki i Techniki, ser. CTS., 1988, N 1, p.54.
13. *Nexen W.E., Turner W.C., Cummins W.F.* Rev. Sci. Instr. 1979, v.50(10), p.1227.
14. *Meek J.M., Craggs J.D.* Electrical Breakdown of Gases. Oxford, Clarendon Press, 1953.

15. *Thompson M.W.* Phil. Mag., 1968, v.18. p.377.
16. *Mertens Ph., Bogen P.* Journal of Nucl. Mat., 1984, v.128-129, p.551.
17. *Galeev A.A., Sagdeev R.S.* Fizika Plazmy, 1983, v.9(1), p.209.
18. *Vasil'ev N.N., Lukash V.E., Bekhtenev A.A. et al.* Voprosy Atomnoy Nauki i Techniki, ser. CTS., 1985, N 2, p.41.

G.F. Abdrashitov, A.V. Beloborodov, V.I. Volosov, V.V. Kubarev, Yu.S. Popov, Yu.N. Yudin

Hot Rotating Plasma (PSP-2 Experiment)

Г.Ф. Абдрашитов, А.В. Белобородов, В.И. Волосов, В.В. Кубарев, Ю.С. Попов, Ю.Н. Юдин

Горячая вращающаяся плазма (эксперимент ПСП-2)

Ответственный за выпуск С.Г.Попов

Работа поступила 17 марта 1989 г.
Подписано в печать 18.07 1989 г. МН 12099.
Формат бумаги 60×90 1/16 Объем 2,9 печ.л., 2,4 уч.-изд.л.
Тираж 290 экз. Бесплатно. Заказ № 86.

Набрано в автоматизированной системе на базе фотонаборного автомата ФА1000 и ЭВМ «Электроника» и отпечатано на ротапринте Института ядерной физики СО АН СССР,
Новосибирск, 630090, пр. академика Лаврентьева, 11.